Intersubunit Interactions Associated with Tyr42α Stabilize the Quaternary-T Tetramer but Are Not Major Quaternary Constraints in Deoxyhemoglobin[†,‡]

Jeffrey S. Kavanaugh,[§] Paul H. Rogers, and Arthur Arnone

Department of Biochemistry, Roy J. and Lucille A. Carver College of Medicine, The University of Iowa, Iowa City, Iowa 52242

Hilda L. Hui, Anita Wierzba, Alice DeYoung, Laura D. Kwiatkowski, and Robert W. Noble

Department of Medicine, University at Buffalo, Department of Veterans Affairs Medical Center, Buffalo, New York 14215

Laura J. Juszczak,[§] Eric S. Peterson,[||] and Joel M. Friedman*

Department of Physiology and Biophysics, Albert Einstein College of Medicine, Bronx, New York 10461

Received July 19, 2004; Revised Manuscript Received December 30, 2004

ABSTRACT: Previous mutational studies on Tyr42α variants as well as the current studies on the mutant hemoglobin αY42A show that the intersubunit interactions associated with Tyr42α significantly stabilize the α1β2 interface of the quaternary-T deoxyhemoglobin tetramer. However, crystallographic studies, UV and visible resonance Raman spectroscopy, CO combination kinetic measurements, and oxygen binding measurements on αY42A show that the intersubunit interactions formed by Tyr42α have only a modest influence on the structural properties and ligand affinity of the deoxyhemoglobin tetramer. Therefore, the α1β2 interface interactions associated with Tyr42α do not contribute significantly to the quaternary constraints that are responsible for the low oxygen affinity of deoxyhemoglobin. The slight increase in the ligand affinity of deoxy αY42A correlates with small, mutation-induced structural changes that perturb the environment of Trp37β, a critical region of the quaternary-T α1β2 interface that has been shown to be the major source of quaternary constraint in deoxyhemoglobin.

The quaternary structure of the $\alpha_2\beta_2$ hemoglobin tetramer, an assembly of two identical $\alpha\beta$ dimers, is very sensitive to ligation state. Several high-resolution crystallographic studies have shown that fully deoxygenated hemoglobin has virtually the same quaternary structure, the T quaternary structure, under high-salt and low-salt crystallization conditions (*1*−*3*). In contrast, fully liganded hemoglobin is characterized by an ensemble, the R^e ensemble, of energetically similar but spatially distinct quaternary structures.[1] Formation of the quaternary-T dimer−dimer interface in deoxyhemoglobin dramatically decreases the oxygen affinity of the α- and β-subunits several hundred-fold and results in a tetramer that exhibits positive cooperativity. Thus, at least some of the intersubunit interactions that define the quaternary-T dimer−dimer interface must function as "quaternary constraints" that inhibit the binding of oxygen to the α- and β-heme groups of the deoxygenated T quaternary state by opposing ligand-induced changes in T state structure. The classic two-state model of Monod, Wyman, and Changeux (*8*) states that initial ligand binding weakens the quaternary-T constraints and shifts the T−R^e equilibrium in favor of the R^e ensemble. In contrast, recent thermodynamic studies by Ackers et al. (*9*) suggest that the initial events associated with ligand binding disrupt quaternary-T constraints such that partially liganded hemoglobin adopts a high-affinity T-like structure. In particular, the data of Ackers et al. (*9*) reveal the existence of intradimer cooperativity within the T-like tetramer; i.e., binding a ligand to an α- or β-subunit disrupts quaternary constraints associated with the unliganded subunit on the same $\alpha\beta$ dimer, increasing its ligand affinity. Identifying the quaternary-T constraints and determining how liganded binding disrupts them are central to understanding hemoglobin's mechanism.

Tyr42α forms an intersubunit hydrogen bond with Asp99β across the dimer−dimer interface in the quaternary-T tetramer, but not in the R^e ensemble (*4*, *10*). Therefore, this interaction was a reasonable candidate for an important quaternary-T constraint. Early support for this assignment came from studies on β99 mutants where a marked desta-

[†] This work was supported by National Institutes of Health Program Project Grant PO1 GM-58890.

[‡] Refined coordinates and structure factors for deoxyhemoglobin A and deoxy αY42A have been deposited in the RCSB Protein Data Bank. The access codes for deoxyhemoglobin A and deoxy αY42A are 1RQ3 and 1XZ2 in crystal form 1, respectively, and 1XYE and 1XZ4 in crystal form 2, respectively.

* To whom correspondence should be addressed. Telephone: (718) 430-3591. Fax: (718) 430-8819. E-mail: jfriedma@aecom.yu.edu.

[§] Both authors are to be considered as the first author.

[||] Present address: Department of Chemistry, Bowdoin College, Brunswick, ME 04011-8466.

[1] Recent crystallographic studies have shown that fully liganded hemoglobin adopts an ensemble of energetically accessible structures (*4*). The structures in this ensemble are spatially distributed over a range that varies between the quaternary-R (*5*) and quaternary-R2 (*6*) conformations. The symbol R^e refers to this ensemble. Very recent NMR experiments have shown that the quaternary structure of liganded hemoglobin in solution also is best represented by an ensemble of energetically similar conformations with the average structure midway between the R and R2 conformations (*7*). In this paper, reference to the R^e ensemble is synonymous with the term R-state used in most previous publications.

10.1021/bi0484670 CCC: $30.25
Published on Web 02/16/2005

bilization of the quaternary-T structure has been attributed to the absence of the Tyr42α−Asp99*β* hydrogen bond (*11*, *12*). In the absence of potent allosteric effectors, many of these mutants are noncooperative, and it has been suggested that they are locked in the R^e ensemble even when fully deoxygenated. The restoration of cooperativity in the noncooperative *β*D99N mutant, Hb Kempsey, as the result of a second, compensatory αY42D mutation also has been cited as evidence of the critical nature of the Tyr42α−Asp99*β* hydrogen bond in wild-type deoxyhemoglobin (*13*, *14*). Similarly, studies on the αY42F and αY42H mutants also yielded evidence in favor of the purported critical role played by the Tyr42α−Asp99*β* hydrogen bond. The key observation was that the noncooperative phenylalanine mutant cannot form the hydrogen bond whereas the cooperative histidine mutant is capable of forming the hydrogen bond, albeit at a much weaker level than in the wild-type protein (*15*−*18*). However, these results link the Tyr42α−Asp99*β* hydrogen bond only to the stability but not to the ligand affinity or to the conformation of the T state.

In the study presented here, the αY42A[2] mutant is studied and compared to the previously studied α42 mutants mentioned above. The replacement of tyrosine with the nonpolar alanine residue eliminates the potential for the hydrogen bond and introduces a nonpolar side chain that is much smaller and less interactive than amino acid side chains in the other two α42 mutants. Here we report X-ray crystallographic studies, visible and UV resonance Raman spectroscopic studies, and functional studies that show the deoxygenated αY42A mutant can form a quaternary-T tetramer, which both manifests key conformational elements associated with quaternary constraint and binds the ligand with only a moderately greater affinity than the deoxygenated T state of HbA. However, the removal of the phenolic group at α42 by the Ala substitution substantially destabilizes the deoxygenated T state, reducing the equilibrium constant for the assembly of two α*β* dimers into a deoxygenated tetramer by 2000-fold. Unlike the αY42F variant, the αY42A variant binds oxygen cooperatively with an overall increase in affinity of only 3-fold. Therefore, the Tyr42α−Asp99*β* hydrogen bond and the other interactions associated with the phenolic side chain of Tyr42α make major contributions to the stability, but not the quaternary constraint, of the T quaternary structure of hemoglobin.

MATERIALS AND METHODS

Synthesis of the αY42A Mutant Hemoglobin. The αY42A mutation was created by cassette mutagenesis using a modified form of pUC18 in which a synthetic α-globin gene that uses optimum *Escherichia coli* codons was cloned between the XbaI and PstI sites of the polylinker region. The other restriction endonuclease recognition sites in the linker region of this plasmid (which was provided by R. Hernan and S. Sligar, University of Illinois, Urbana, IL) were eliminated to facilitate cassette mutagenesis. The αY42A mutation was introduced by replacing the AflII−BamHI cassette, which corresponds to α-globin residues 33−52, with a cassette that encoded alanine at position 42α. After transformation into competent DH5α cells, automated DNA sequencing (done at The University of Iowa College of Medicine DNA Core Facility) was used to identify plasmids that contained the αY42A mutation. The mutated α-globin gene was then cloned into the region between the XbaI and PstI sites of the pUC18-based α/*β* coexpression vector described by Hernan et al. (*19*). Constitutive coexpression of the α- and *β*-globin genes in *E. coli* strain TB-1 did not produce sufficient quantities of the mutant hemoglobins; 136 L of bacterial culture yielded approximately 20 mg of tetrameric hemoglobin. Yields were increased significantly by cloning the entire α/*β*-globin operon into the T7 expression plasmid pET17b (Novagen, Madison, WI). Transformed *E. coli* strain BL21(DE3) was grown at 37 °C in LB medium (1 L of culture per 2.8 L Fernbach flask) containing 100 mg/mL ampicillin for 36 h with gentle shaking (∼60 rpm). The cells were not induced with IPTG because induction resulted in lower hemoglobin production. The mutant α-globin was isolated from the expressed hemoglobin, and a functionally homogeneous mutant hemoglobin was assembled from normal human *β*-subunits, the α-globin, and hemin as described by Hui et al. (*20*). It should be noted that the αY42A hemoglobin also contains the αV1M mutation. Hui et al. (*20*) recently demonstrated that the αV1M mutation has no significant effect on the structural or functional properties of hemoglobin.

Cross-Linking the αY42A Mutant between Lys99α1 and Lys99α2. In the past, we prepared *β*-chain mutants cross-linked between residues Lys99α1 and Lys99α2 by combining the mutant *β*-globin with hemin and cross-linked αα dimers (*21*). This method is unsuitable for the preparation of cross-linked α-chain mutants. Instead, the cross-linking reaction was carried out after preparation of the mutant hemoglobin from the α-globin, heme, and normal *β*-subunits. The cross-linking procedure was based on that of Chatterjee et al. (*22*) and Snyder et al. (*23*), as described by Kwiatkowski et al. (*21*), but the scale was greatly reduced. A total of 13 mg of the αY42A mutant was concentrated to 1.6 mM in heme in 50 mM HCl bis-Tris (pH 7.2), and a 5-fold molar excess of IHP over Hb tetramer was added. This solution was deoxygenated for 1 h on ice under a nitrogen atmosphere and then placed in a 37 °C water bath for 15 min. An equal volume of deoxygenated 0.5 mM DBF in 0.2 M Hepes buffer (pH 7.2) was added anaerobically, and the reaction mixture was incubated for 2 h with continuous gentle shaking for the last hour. The reaction was then stopped by the addition of 1 M glycine (pH 9) to a final concentration of 0.2 M. The reaction mixture was kept at 37 °C for an additional 15 min and then placed on ice. After reaching 4 °C, the reaction mixture was quickly reoxygenated by being exposed to air. The reaction mixture was then filtered through a G-25F column equilibrated with 1 mM HCl Tris (pH 8.2), deionized by being passed through a Dintzis column (*24*), and fractionated by HPLC as previously described (*21*).

Kinetics of CO Combination with Deoxygenated Hemoglobin. These kinetics were measured with an OLIS (On Line Instrument Systems Inc., Bogart, GA) USA stopped flow apparatus as described by Doyle et al. (*25*). Reactions were followed at 420 and 435 nm using a 1.7 cm path length cell at pH 7 and 20 °C. Concentrations of CO and hemoglobin (in heme equivalents) were 20 and 2 *μ*M, respectively.

[2] Abbreviations: PEG, polyethylene glycol; αY42A, recombinant hemoglobin with the Tyr42α → Ala and Val1α → Met mutations.

Oxygen Equilibrium Measurements. These were carried out tonometrically as previously described (*26*). A 500 mL tonometer with an attached 2 mm cuvette was used. The Hb concentration was 200 μM in heme equivalents. Spectral measurements were carried out in a Cary 14 spectrophotometer modified by OLIS for computer control and on-line data acquisition. For these measurements, solutions contained, in addition to buffer and hemoglobin, the ferredoxin NADP reductase system of Hayashi et al. (*27*) for maintenance of the heme groups in their ferrous state.

Visible Resonance Raman Spectra. The resonance Raman spectra of the equilibrium deoxy derivatives and the photoproducts of the CO-bound derivatives of HbA and αY42A were obtained using a Raman apparatus described in detail in ref *28*. Briefly, Soret band-enhanced time-resolved Raman spectra were obtained using an 8 ns, 150 μJ, 435.8 nm pulse to both photodissociate the ligand (in the case of the CO derivatives) and to generate Raman scattering from the sample. A frequency-doubled Nd:YAG laser (NY81C-20, Continuum, Santa Clara, CA) that was frequency shifted via stimulated Raman scattering in a hydrogen cell was used. The detector was an intensified diode array run in the CW mode (P/N IRY-1024S/B, Princeton Instruments, Trenton, NJ). The spectral bandwidth of the monochromator was approximately 2.5 cm^{-1}, and the resolution of the detector array was approximately 0.9 cm^{-1} per pixel. Raman spectra were calibrated using solvent spectra with previously determined peak assignments. A least-squares fit was used to map the pixel number onto relative wavenumbers (Raman shift), and the resulting Raman shift values are estimated to be accurate to within ± 0.25 cm^{-1}. The Raman spectra were baselined using a polynomial fitting routine in LabCalc (Galactic Industries, Salem, NH), were normalized in intensity using the ν_7 mode band at $\sim$672 cm^{-1}, and are presented without smoothing. In this study, the sample was contained in either a spinning NMR tube or a special disk-shaped holder described previously (*28*). The focus in this study was on the low-frequency portion of the Raman spectrum which contains ν(Fe−His), the iron−proximal histidine stretching mode. This Raman band is especially sensitive to both quaternary and tertiary conformation changes (*28*−*38*).

UV Resonance Raman Spectra. The CW UV resonance Raman spectra of the deoxy and CO-bound derivatives of HbA and αY42A were generated using the 229 nm output of a frequency-doubled argon ion laser (1.8 mW at the sample). The Raman scattered light was collected, dispersed, and detected using a previously described (*14*, *39*−*41*) UV Raman apparatus derived from a single spectrograph with a CCD detector. As in previous UV Raman studies, the 934 cm^{-1} perchlorate band is used as an internal Raman intensity standard.

Sample Preparation for Raman Measurements and Sample Integrity. Both the UV and visible resonance Raman measurements utilized solution samples that were 0.8 mM in heme at pH 7.5 (50 mM potassium phosphate buffer). When IHP was present, its concentration was 5-fold greater than that of the Hb tetramer. The samples also contained 0.3 M sodium perchlorate for use as an internal Raman intensity standard for the UV Raman measurements.

The oxidation state, degree of ligation, and degree of degradation were determined by measuring the absorption spectra of samples before and after each data acquisition on a Perkin-Elmer UV−vis spectrometer. A protocol was developed that allowed for the generation of the absorption spectrum from small volumes of the sample within NMR tubes.

Crystal Growth. Prior to crystallization, the αY42A mutant hemoglobin was stripped of organic and inorganic ions by being passed over a Dintzis column (*24*) that was modified by the addition of a 1 mm layer of chelating resin (iminodiacetic acid, Sigma catalog no. C-7901) to the top of the column. The stripped oxyhemoglobin was frozen and stored in liquid nitrogen until it was used for crystallization. Thawed oxyhemoglobin solutions and all of the crystallization stock solutions were thoroughly deoxygenated before use, and all crystallization work was conducted in a glovebag that was continuously purged with nitrogen.

Crystals of deoxyhemoglobin are typically grown from concentrated solutions of ammonium sulfate as described by Perutz (*42*) or from PEG solutions as first described by Ward et al. (*43*). The monoclinic crystals that grow from ammonium sulfate solutions are often termed "high-salt" crystals, and the orthorhombic crystals that grow form PEG solutions are often termed "low-salt" crystals. Although the high-salt conditions failed to produce crystals of the deoxy αY42A mutant, crystals were obtained using the low-salt crystallization conditions. Specifically, crystals were grown in 100 μL batch setups at room temperature from solutions containing 10 mg/mL Hb, 10 mM ammonium phosphate (pH 7.0), 100 mM potassium chloride, 3 mM sodium dithionite, and 10−10.5% PEG 6000. Each vial was seeded with a small deoxy HbA crystal as previously described (*2*). Although the resulting crystals appeared to be well-formed and were isomorphous with low-salt deoxy HbA crystals (crystal form 1 in Table 1), they did not diffract as well as the typical crystals of wild-type or other mutant hemoglobins that grow from the low-salt conditions (see below).

After the standard high- and low-salt crystallization protocols failed to yield high-quality crystals of deoxy αY42A, alternative crystallization conditions were explored. Crystal Screen 1 (*44*) and Crystal Screen 2 (*45*) kits (Hampton Research, Laguna Niguel, CA) were used to carry out 20 μL batch setups in which the hemoglobin concentration was 20 mg/mL and the concentration of the crystallization reagent was 80% of the published concentration. Each vial also contained 3 mM sodium dithionite for maintenance of the iron atoms in the ferrous state. For crystallization reagents that gave promising results, 100 μL batch setups in which the concentration of the crystallization reagent was varied were created.

Well-ordered crystals that diffracted to 2.0 Å resolution were obtained using Crystal Screen 1 reagent 10. Crystals grew best when the concentration of reagent 10 was 50% of its stock concentration; i.e., crystals grew from solutions containing 15% PEG 4000, 50 mM sodium acetate (pH 4.6), 100 mM ammonium acetate, 20 mg/mL αY42A, and 3 mM sodium dithionite. These crystals were not isomorphous with either the high- or low-salt crystal forms of deoxyhemoglobin, but they were isomorphous with wild-type deoxy HbA crystals grown from very low ionic strength solutions containing 12−14% PEG 1450 [N.-L. Chan and A. Arnone, unpublished results; Kavanaugh et al. (*46*); crystal form 2 in Table 1].

Table 1: Data Collection and Refinement Statistics[a]

parameter	deoxy HbA crystal form 1	deoxy αY42A crystal form 1	deoxy HbA crystal form 2	deoxy αY42A crystal form 2
PDB code	1RQ3	1XYE	1XZ2	1XZ4
		Data Collection		
space group	$P2_12_12$	$P2_12_12$	$P2_12_12_1$	$P2_12_12_1$
unit cell				
a (Å)	97.0	97.0	83.9	84.1
b (Å)	99.3	99.3	112.1	111.9
c (Å)	66.0	66.2	83.9	84.1
asymmetric unit	tetramer	tetramer	tetramer	tetramer
resolution (Å)	1.91 (2.05−1.91)	2.13 (2.29−2.13)	1.93 (2.07−1.93)	1.98 (2.13−1.98)
no. of measurements	185171 (21386)	243449 (19998)	400584 (43454)	229703 (20613)
no. of unique reflections	47999 (7770)	36379 (6440)	44690 (7546)	41133 (7049)
completeness (%)	95.3 (78.1)	97.9 (90.2)	96.6 (83.2)	96.7 (84.1)
average $I/\sigma(I)$	13.7 (3.0)	5.4 (1.3)	12.4 (2.9)	9.8 (1.7)
average multiplicity	6.7 (2.8)	6.7 (3.1)	9.0 (5.8)	6.5 (2.9)
R_{merge} (%)	4.4 (14.9)	15.3 (29.9)	5.9 (18.5)	6.5 (24.2)
		REFMAC5 Refinement		
R_{cryst}	0.165 (0.212)	0.192 (0.279)	0.168 (0.197)	0.183 (0.248)
R_{free}	0.198 (0.249)	0.241 (0.328)	0.201 (0.243)	0.224 (0.288)
rms for bond lengths (Å)	0.018	0.021	0.014	0.020
rms for bond angles (deg)	1.84	1.97	1.49	1.89
average *B* factor (Å^2)	24.8	19.7	19.7	25.0

[a] Values in parentheses are for the highest resolution shell of data. Refinement statistics are for the models obtained when reflections in test set "zero" were excluded for the refinement.

Collection of X-ray Diffraction Data. All X-ray diffraction data were collected on a Rigaku AFC6 diffractometer fitted with a San Diego Multiwire Systems area detector, and all data were scaled and merged according to the procedure of Howard et al. (*47*). The low-salt deoxy αY42A crystals were washed in a substitute mother liquor containing 13% PEG 6000 and mounted in quartz capillary tubes prior to data collection. Although (as mentioned above) most of these crystals did not diffract well, one crystal diffracted reasonably well to 2.0 Å resolution, but the R_{symm} statistic was rather high at 15.3% (Table 1).

Crystals of deoxy αY42A in crystal form 2 were washed briefly in a substitute mother liquor of 15% PEG 4000 containing fresh sodium dithionite and then mounted in quartz capillaries. The crystals diffracted well to 1.98 Å resolution with an R_{symm} of 6.5% (Table 1).

Refinement and Cross-Validation of the Structural Changes in αY42A in Crystal Forms 1 and 2. The crystal structures of deoxy αY42A in crystal forms 1 and 2 were refined and the mutation-induced structural changes validated using the protocols recently described by Chan et al. (*48*). In brief, each native deoxy HbA diffraction data set (i.e., data sets from crystal forms 1 and 2) was randomly divided into 10 mutually exclusive test data sets consisting of 10% of the data and working data sets consisting of the remaining 90% of the data. The corresponding deoxy αY42A diffraction data for crystal forms 1 and 2 were assigned to the same test and working data sets on the basis of their Miller indices. For each crystal form, 10 native deoxy HbA atomic models were debiased (*49*) relative to the 10 test data sets by carrying out more than 600 cycles of maximum-likelihood refinement using REFMAC5 (*50*, *51*). Each deoxy HbA model (that had been debiased relative to a particular test data set) was then used as a starting model (with Tyr42α converted to an alanine residue)[3] for the refinement of deoxy αY42A in crystal forms 1 and 2 (10 atomic models for each crystal form). These refinements consisted of rigid-body refinements with X-PLOR (*52*) as described previously (*48*), followed by REFMAC5 refinement and minor manual corrections with the TOM/FRODO software (*53*, *54*). Refinement statistics for deoxy HbA and deoxy αY42A in crystal forms 1 and 2 are listed in Table 1.

The $R_{free}^{local-5}$ statistic (*46*, *48*) then was used to validate the mutation-induced tertiary structure changes in both crystal forms 1 and 2. This statistic uses the unbiased test data sets to cross-validate small tertiary structure differences between wild-type deoxy HbA and αY42A. That is, the localized mutation-induced changes in tertiary structure that were introduced during the second stage of the refinement (the REFMAC5 and TOM/FRODO refinement) were cross-validated through the use of "hybrid" atomic models. Specifically, after convergence of the final REFMAC5 refinement cycles, hybrid atomic models were generated by replacing the coordinates of each pentapeptide in the final REFMAC5 refined model with the coordinates of the corresponding pentapeptide of the atomic model that had undergone only rigid-body refinement (but not individual atom refinement). The coordinates for each of these hybrid models were identical to those of the final refined model except for a single (unrefined) pentapeptide. The standard R_{free} value (*55*) calculated with a particular hybrid model minus the standard R_{free} value calculated with the final atomic model is defined as the $R_{free}^{local-5}$ value associated with the replaced pentapeptide. If the structural changes associated with a particular pentapeptide represent a genuine improvement to the starting model, the corresponding $R_{free}^{local-5}$ value should be significantly greater than zero. Because the $R_{free}^{local-5}$ value is a statistic that is sensitive only to structural changes in a particular peptide, it can be used to discriminate between small genuine structural changes and those changes

[3] Due to differences in amino-terminal processing in *E. coli* and humans, this recombinant protein also has an innocuous αV1M mutation (*20*). H*o*wever, residue Met1α was modeled as an alanine residue because the side chain atoms are disordered and not visible in electron density images.

in the atomic model that are due to experimental uncertainty (i.e., uncertainty associated with poorly defined regions of the electron density map).

When the individual $R_{free}^{local-5}$ values are plotted versus residue number, a $R_{free}^{local-5}$ profile is generated that can be compared with a corresponding $rmsd_5$ profile of the root-mean-square tertiary structure differences (see below) between the two structures being analyzed. Peaks in the $R_{free}^{local-5}$ profile identify (cross-validate) significant differences in tertiary structure. By averaging all 10 $R_{free}^{local-5}$ profiles (one for each of the 10 test data sets) to generate a $\langle R_{free}^{local-5} \rangle$ profile, we use all the diffraction data to cross-validate the observed tertiary structure changes.

Analysis of Crystal Structures. To identify mutation-induced changes in tertiary structure, corresponding subunits of deoxy HbA and αY42A were superimposed using an iterative least-squares superposition ("sieve-fit") procedure (*4*, *46*) similar to that described by Gerstein and Chothia (*56*). Changes in tertiary structure were identified by calculating the root-mean-square deviation (rmsd) of all the atoms (backbone and side chain atoms) for each pair of corresponding pentapeptides in the superimposed subunits. This statistic, termed $rmsd_5$, is plotted versus residue number to generate a profile of the five-residue averaged tertiary structure changes. A five-residue window was selected so that the $rmsd_5$ values corresponded with the $R_{free}^{local-5}$ values (above). Mutation-induced changes in quaternary structure were analyzed using methods originally described by Cox (*57*) and more recently by Mueser et al. (*4*) and Kavanaugh et al. (*46*).

RESULTS

CO Combination Kinetics. The time courses for the combination of CO with deoxy HbA and deoxy αY42A at pH 7 in the absence and presence of 100 μM IHP were compared. The results are shown in Figure 1. The kinetics of combination of CO with cross-linked αY42A are also presented. As previously demonstrated [see Figure 6 of Fowler et al. (*58*)], cross-linking HbA has little effect on the kinetics of CO combination with the unliganded protein either in the absence or in the presence of IHP. As expected, CO combines with deoxy HbA with accelerating kinetics both in the absence and in the presence of IHP, the effect of the latter being to slow the combination reaction by a factor of roughly 2. On the other hand, CO combines with deoxy αY42A in the absence of IHP in two easily distinguished kinetic phases, a small, rapid reaction followed by a much larger, relatively slow reaction. Cross-linking the αY42A variant eliminates the initial fast kinetic phase in CO combination and yields a markedly autocatalytic time course for the reaction. Addition of 100 μM IHP to un-cross-linked αY42A also eliminates the rapid kinetic phase, again resulting in an accelerating kinetic process. IHP addition also slows the overall reaction considerably.

As previously reported (*25*), the biphasic reaction of CO with the deoxy αY42A variant in the absence of IHP can be fitted to a sum of two exponential functions. As presented in Table 2, the rapid process was found to represent roughly 10% of the total reaction with an average second-order rate constant of 7 μM^{-1} s^{-1}. At the same time, approximately 90% of the reaction occurs with an average rate constant of 0.52 μM^{-1} s^{-1}. The smaller, rapid process is consistent with the presence of free $\alpha\beta$ dimers. The slower rate constant is indicative of a quaternary-T tetramer with a greater than normal rate of ligand binding and therefore consistent with an increased ligand affinity. Nonetheless, this slower rate constant is well below those of either dimers or quaternary-R^e hemoglobin tetramers.

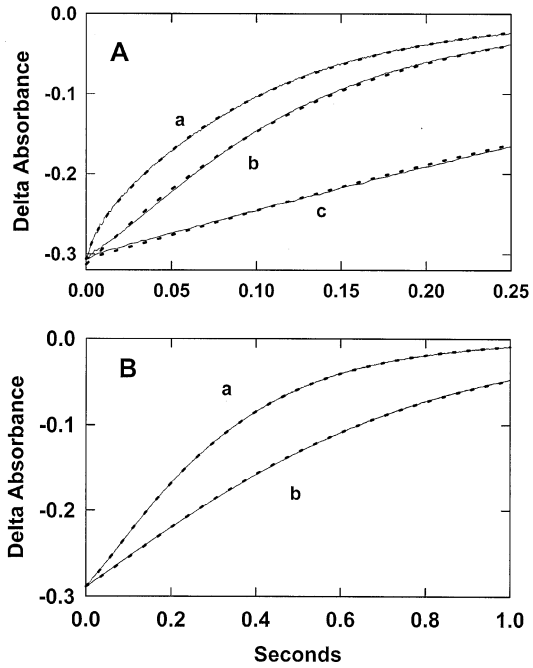

FIGURE 1: Time courses for the combination of CO with the αY42A variant of human hemoglobin and with human HbA at pH 7 and 20 °C. The solid lines show the change in absorbance at 420 nm as a function of time. In panel A, the reaction with αY42A was examined in the absence (curve a) and presence (curve c) of 100 μM IHP. The reaction was also examined in the absence of IHP for the αY42A variant which had been cross-linked between its lysine α99 residues (curve b). In panel B, the reaction of HbA was also assessed in the absence (curve a) and presence (curve b) of 100 μM IHP. Note the difference in the two time scales. The results of the fittings of these curves are displayed by the elongated points which follow the data lines. Curve a of panel A was fitted to the sum of two exponential functions. All other curves were fitted to a two-step sequential process.

Table 2: Results of Single-Exponential and Sequential Fits to CO Combination Data

hemoglobin	IHP	l' (μM^{-1} s^{-1})	l'_{init} (μM^{-1} s^{-1})	l'_{fin} (μM^{-1} s^{-1})	l'_{fin}/l'_{init}
HbA	−	0.17	0.11	0.37	3.3
HbA	+	0.09	0.06	0.15	2.5
αY42A	−	7.0[a]			
		0.52[a]			
αY42A	+	0.16	0.10	0.30	3.0
αY42AXL99α	−	0.43	0.32	0.57	1.8

[a] This is a biphasic CO combination process as described in the text.

If the accelerating reactions are fitted to single-exponential functions, one obtains an estimate of the overall rate of the reaction, but the data are not well fitted. However, sums of exponential functions cannot give meaningful fits to such time courses. As previously reported (*25*), such data can be fitted to a two-step sequential process:

$$Hb + 4CO \xrightarrow{2l'_{init}} Hb(CO)_2 + 2CO \xrightarrow{l'_{fin}} Hb(CO)_4$$

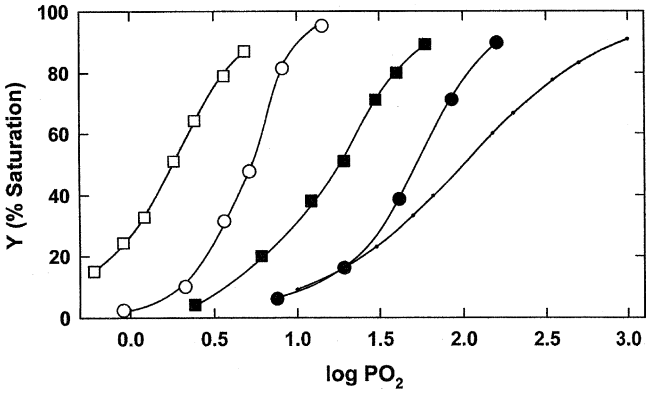

FIGURE 2: Oxygenation isotherms for HbA (□), HbA and 100 μM IHP (○), αY42A (■), and αY42A and 100 μM IHP (●). Measurements were carried out at 20 °C in 100 mM chloride bisTris buffer (pH 7). The solid line on the right indicates a binding curve with a Hill coefficient of unity.

No claim is made that such a representation adequately describes the kinetics of binding of CO to hemoglobin. However, this procedure yields reasonably good fits to the data, and the ratio of l'_{fin} to l'_{init} offers a convenient measure of autocatalysis. Furthermore, l'_{init} has been shown to be closely correlated with oxygen affinity of the low-affinity T quaternary state in the presence of IHP (*59*−*61*). The second-order rate constants obtained from fittings to single-exponential functions, l', and to two sequential processes, l'_{init} and l'_{fin}, are reported in Table 2.

In the absence of IHP, the l'_{fin}/l'_{init} ratio for HbA is roughly 3. The addition of IHP reduces the rate of binding of CO to HbA, and in general lowers the l'_{fin}/l'_{init} ratio. The sequential fit to the accelerating reaction observed with αY42A in the presence of IHP indicates a l'_{fin}/l'_{init} ratio of 3. The apparent rate constants associated with l'_{fin} and l'_{init} are significantly greater than those for HbA under the same experimental conditions, and in the presence of IHP actually approximate those of HbA in the absence of IHP. The sequential fit to the accelerating kinetics of the reaction of CO with cross-linked αY42A in the absence of IHP gives an l'_{fin}/l'_{init} ratio of 1.8, and the l'_{fin} and l'_{init} values are again significantly greater than those for HbA under the same experimental conditions.

The apparent difference in the values of l' for tetrameric, un-cross-linked αY42A, and cross-linked αY42A probably results from the presence of rapidly reacting dimers in the former case. The effect of the initial rapid kinetic reaction is to mask the slower portion of the accelerating reaction of CO with the Hb tetramer. This has two effects. It results in an overly high estimate of the rate for the rapid phase, and skews the estimate of the rate of the slower, tetramer process toward that of the latter portion of the process, l'_{fin}. Therefore, the estimated rate of the tetramer reaction for the un-cross-linked mutant, 0.52 μM^{-1} s^{-1}, is probably most properly compared to l'_{fin} for the cross-linked sample, 0.57 μM^{-1} s^{-1}.

Oxygen Equilibrium Measurements. In Figure 2, fractional saturation with oxygen is plotted as a function of log PO_2 for HbA and the αY42A variant at pH 7 and 20 °C in the presence and absence of 100 μM IHP. As listed in Table 3, in both the presence and absence of IHP, the oxygen partial pressure required for half-saturation of the αY42A mutant is some 3-fold lower than that for HbA. This increase in oxygen affinity is accompanied by a decrease in overall cooperativity in the absence of IHP, but in the presence of IHP, the effect of the mutation on cooperativity appears to be negligible.

Table 3: Oxygen Equilibrium Data in the Presence and Absence of 100 μM IHP[a]

hemoglobin	IHP	P_{50} (mmHg)	n_{max}
HbA	−	4.9	2.9
αY42A	−	1.8	1.9
HbA	+	52	1.8
αY42A	+	17	1.6

[a] Conditions: 100 mM Cl^-, Bis Tris, pH 7, 20 °C, and [Hb] = 200 μM.

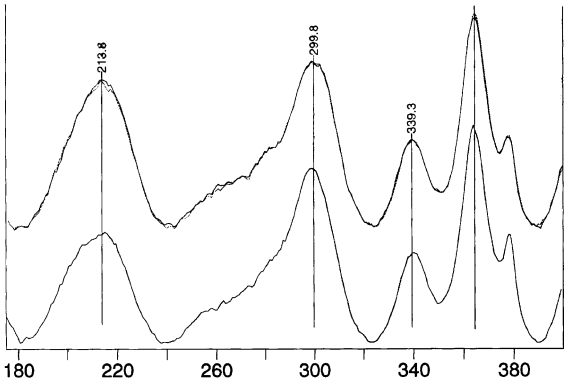

FIGURE 3: Low-frequency region of the Soret-enhanced resonance Raman spectrum of deoxy HbA (bottom) and deoxy αY42A with and without added IHP (top). The peak at ∼214 cm^{-1} arises from ν(Fe−His), the iron−proximal histidine stretching mode.

Visible Resonance Raman Spectra. Figure 3 shows a comparison of the low-frequency portion of the Soret-enhanced resonance Raman spectra of deoxy HbA and deoxy αY42A. The frequencies of all the observed Raman bands, including ν(Fe−His), are almost identical for the deoxy derivatives of HbA (bottom) and αY42A (top) in both the presence and absence of IHP (5-fold excess over tetramer). Figure 4 shows a blowup of the iron−proximal histidine stretching mode, ν(Fe−His). It is observed that for both species, the spectrum is minimally sensitive to the addition of IHP; however, as can be seen in Figure 4, there is a slight difference in the band profile of ν(Fe−His) when comparing the two samples. The band for deoxy αY42A is skewed slightly toward higher frequencies (dark and light solid lines) compared to that of deoxy HbA (dashed line). This difference is seen both with and without IHP. The primary cause of the difference appears to arise from the low-frequency shoulder that is known to be derived from the heme contribution of the α-chains. Deoxy derivatives of Hbs that are likely to yield detectable concentrations of dimer such as certain β37 mutants (*28*) yield frequencies that are significantly elevated compared to those reported above.

UV Resonance Raman Spectra. The high-frequency region of the 229 nm excited UV resonance Raman spectrum from hemoglobin contains bands that have been well characterized with respect to conformational degrees of freedom related to allostery. The weak band at ∼1512 cm^{-1} has recently been reassigned as the 2xW18 overtone mode (*62*). This band shows a decrease in intensity when HbA switches from the deoxy state to the fully liganded state (*32*, *63*−*65*). This

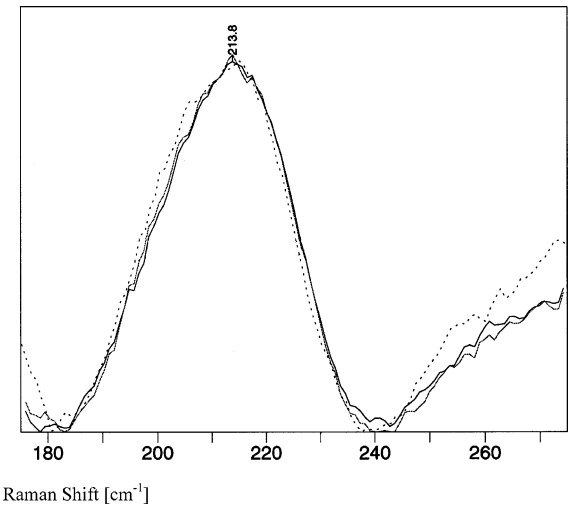

FIGURE 4: Blowup of the ν(Fe−His) Raman bands for deoxy HbA (···) and deoxy αY42A with and without added IHP (—) showing a small frequency difference between the two proteins. The other low frequency Raman bands occurred at exactly the same position for the two deoxy derivatives as reflected in a precise overlap of all the Raman bands shown in Figure 3 with the exception of the ν(Fe−His) band.

intensity change is related to Trp37β in the $\alpha_1\beta_2$ interface based on this band's behavior in the βW37E mutant (*66*). The W3 band at ∼1558 cm^{-1} has two contributions (*36*, *63*, *64*, *67*, *68*). The central feature that peaks at ∼1558 cm^{-1} is derived from the two A-helix tryptophans (α14 and β15), whereas the ligation-sensitive shoulder at ∼1550 cm^{-1} originates from Trp37β. The intensity of this shoulder is reflective of the ligation-sensitive hinge region of the $\alpha_1\beta_2$ interface. Shifts in the position of the 1558 cm^{-1} band are directly linked to changes in the tryptophan χ_2 dihedral angle. For HbA, the tyrosine-derived Y8a band at ∼1616 cm^{-1} shows an ∼2 cm^{-1} shift to higher frequency when liganded HbA is converted to deoxy HbA (*32*, *63*, *65*, *69*, *70*). This frequency shift originates primarily from Tyr42α in the $\alpha_1\beta_2$ interface (*14*, *63*, *64*, *71*−*73*).

Figures 5 and 6 show comparisons of the 229 nm-excited resonance Raman spectra of deoxy and CO HbA and αY42A. At this excitation wavelength, most if not all of the major features in the spectra are derived from vibrational modes of tyrosine and tryptophan (*74*, *75*). In Figure 5, difference spectra are shown as well as a representative spectrum for COHbA (trace a). Trace b shows the previously reported (*63*−*65*, *70*) deoxy minus liganded (CO) difference spectrum for HbA. Note that in this difference spectrum, the intensity at approximately 1550 cm^{-1} corresponds to the low-frequency shoulder of the W3 band whose main peak is at 1558 cm^{-1}. The corresponding deoxy minus CO difference spectrum for the αY42A mutant shown as trace c is quite similar with respect to W3 at 1550 cm^{-1}, the band at 1511 cm^{-1}, W7 at 1361 cm^{-1}, and W16 at 1011 cm^{-1}. A very noticeable difference between the HbA and αY42A is seen in the region of Y8a at approximately 1616 cm^{-1}. For HbA, a substantial derivative-shaped difference band is observed, whereas for αY42A, the derivative-shaped signal is essentially eliminated with only a small intensity difference remaining. Similarly, the large negative difference band for Y9a at 1178 cm^{-1} is reduced for αY42A. Trace d is the deoxy HbA minus deoxy αY42A difference spectrum. Positive intensity is seen for the Y8a, Y7a, and Y9a tyrosine bands at 1618, 1207, and 1178 cm^{-1}, respectively. A small feature is seen at the W3 low-frequency shoulder, whereas readily discernible features are seen for the W7 Fermi doublet and at W16. The difference at the Fermi doublet is consistent with an intensity increase in the 1360 cm^{-1} peak for αY42A and is indicative of a more hydrophobic environment within the αY42A mutant. The corresponding difference spectrum for the CO-bound derivatives, shown as trace e, is very similar to the deoxy difference spectrum. For both the deoxy and CO derivatives, the changes in the 1512 cm^{-1} band, the W3 band, and the Y8a band are more clearly seen in Figure 6, where a blowup of the high-frequency region of the spectrum is shown.

Analysis of the X-ray Crystal Structures of Deoxy αY42A. In general, single mutations do not induce large changes in protein structure. Since mutation-induced changes in tertiary structure are typically on the order of a few tenths of an angstrom, assessing the validity of these small atomic movements is a challenging problem. One test of the significance of a small change in structure is its reproducibility in crystallographically independent environments in the same crystal lattice (i.e., by making use of noncrystallographic symmetry) or in difference crystal lattices. The $R_{\mathrm{free}}^{\mathrm{local}-5}$ parameter (described above) provides a second, complementary approach to the verification of small changes in tertiary structure. As shown below, very small mutation-induced changes in atomic positions and temperature factors in αY42A are reproduced accurately in the crystallographically independent α1β1 and α2β2 dimers of both crystal forms 1 and 2. These structural perturbations are corroborated by the $\langle R_{\mathrm{free}}^{\mathrm{local}-5}\rangle$ parameter which cross-validates structural changes as small as 0.2 Å.

Shown in Figure 7 are plots of rmsd$_5$ and $\langle R_{\mathrm{free}}^{\mathrm{local}-5}\rangle$ profiles for the α-subunits in crystal form 2 (panels a and b) and crystal form 1 (panels c and d) where each parameter has been calculated over all overlapping five-residue windows. In both crystal forms, the rmsd$_5$ and $\langle R_{\mathrm{free}}^{\mathrm{local}-5}\rangle$ profiles identify two major regions of mutation-induced changes in tertiary structure: feature 1α (pentapeptides centered at residues 39α−48α) and feature 2α (pentapeptides centered at residues 89α−98α). Feature 2α has the largest rmsd$_5$ magnitude, occurs in both crystal forms and in both the crystallographically independent α1 and α2 subunits, and is independently validated by unambiguous peaks in the $\langle R_{\mathrm{free}}^{\mathrm{local}-5}\rangle$ profiles. With regard to feature 1α in crystal form 2 (panels a and b in Figure 7), it has a significant rmsd$_5$ magnitude (albeit slightly smaller than the rmsd$_5$ magnitude of feature 2α) and it occurs in both the crystallographically independent α1 and α2 subunits and is independently validated by an unambiguous peak in crystal form 2 $\langle R_{\mathrm{free}}^{\mathrm{local}-5}\rangle$ profile. Although feature 1α in crystal form 1 does not appear as an obvious rmsd$_5$ peak in panel c of Figure 7, there is a clear $\langle R_{\mathrm{free}}^{\mathrm{local}-5}\rangle$ peak for feature 1α in panel d of Figure 7. Therefore, it is apparent that the $\langle R_{\mathrm{free}}^{\mathrm{local}-5}\rangle$ profile is capable of discriminating very small, valid structural changes (i.e., genuine mutation-induced perturbations) from small rmsd$_5$ fluctuations that are due to random refinement variations. In addition to features 1α and 2α, the rmsd$_5$ and $\langle R_{\mathrm{free}}^{\mathrm{local}-5}\rangle$ profiles in Figure 7 indicate that a minor feature (feature 3α which is located at the α COOH terminus) also may be significant.

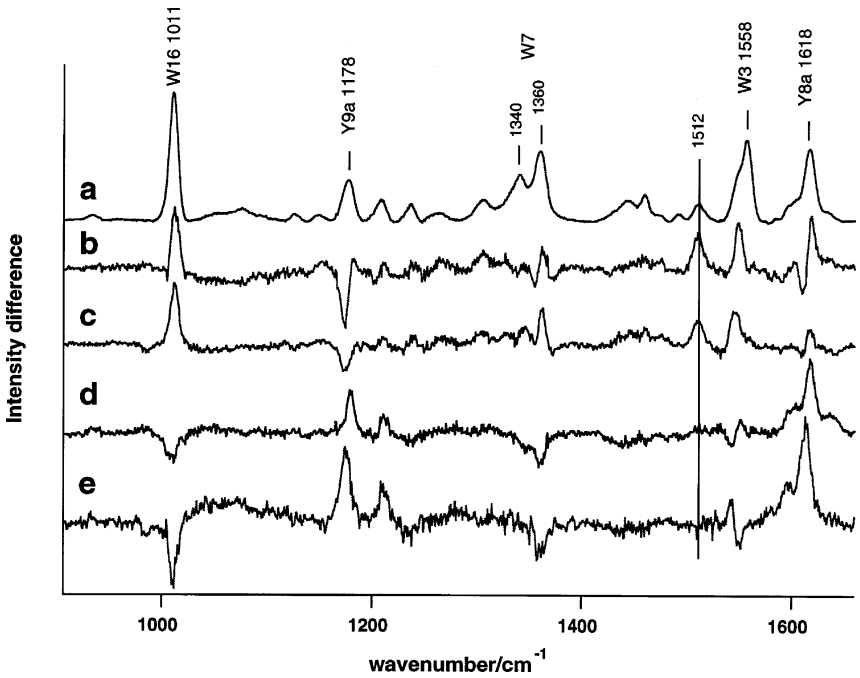

FIGURE 5: Excited (229 nm) UV resonance Raman (UVRR) spectrum of COHbA (a), deoxy CO UVRR difference spectrum for HbA (b), deoxy CO UVRR difference spectrum for αY42A (c), HbA−αY42A UVRR difference spectrum for the deoxy derivatives (d), and HbA−αY42A UVRR difference spectrum for the CO derivatives (e).

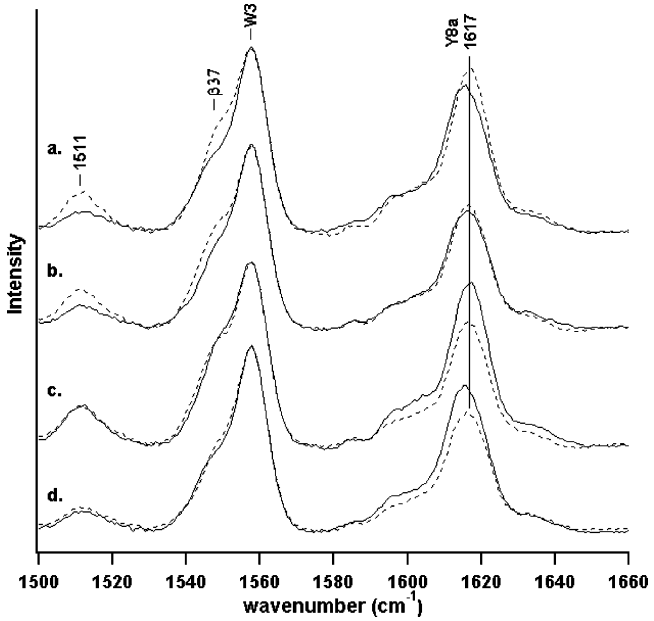

FIGURE 6: High-frequency region of the UVRR spectrum for the deoxy (- - -) and CO (—) derivatives of HbA (a), the deoxy (- - -) and CO (—) derivatives of αY42A (b), the deoxy derivatives of HbA (—) and αY42A (- - -) (c), and the CO derivatives of HbA (—) and αY42A (- - -) (d).

Shown in Figure 8 are plots of rmsd_5 and $\langle R_{\text{free}}^{\text{local}-5}\rangle$ profiles for the β-subunits in crystal form 2 (panels a and b) and crystal form 1 (panels c and d). In both crystal forms, the rmsd_5 and $\langle R_{\text{free}}^{\text{local}-5}\rangle$ profiles identify the same two regions of mutation-induced changes in tertiary structure: region 1β (pentapeptides centered at residues 38β−42β), region 2β (pentapeptides centered at residues 96β−102β). The independent $\langle R_{\text{free}}^{\text{local}-5}\rangle$ profiles from crystal forms 1 and 2 cross-validate very small tertiary structural changes as genuine mutation-induced perturbations. Because the magnitudes of the peaks for features 1β and 2β are near-background levels in the rmsd_5 profiles, their significance would be questionable in the absence of cross-validation by the $\langle R_{\text{free}}^{\text{local}-5}\rangle$ parameter. Moreover, as discussed below, the fact that the β-subunit residues associated with features 1β and 2β are in contact with Tyr42α is further evidence that these very small structural changes are not spurious.

The rmsd_5 and $\langle R_{\text{free}}^{\text{local}-5}\rangle$ profiles in panels a and b of Figure 8 indicate that in crystal form 2 (but not in crystal form 1) a third region of the β-subunits (residues 116β−122β) undergoes a small change in structure. This region is on the surface of β1 and β2 subunits and not associated with the Tyr42α mutation site. Because resides His116β, His117β, and Glu121β are part of this region, the structural change appears to be pH-induced. That is, crystal form 2 crystals of deoxy αY42A and deoxy HbA were grown at pH 4.6 and 7.0, respectively. Thus, residues with side chain pK values between pH 4.6 and 7.0 may have changed their degree of ionization and moved to a new position of equilibrium. (The crystal form 1 crystals of deoxy αY42A and deoxy HbA were both grown at pH 7.0.)

Located at the COOH-terminal end of the C-helix, the side chain Tyr42α interacts with a number of residues that are part of the quaternary-T α1β2 interface (Figure 9). In particular, the hydroxyl group of Tyr42α1 makes a tight intersubunit polar contact 2.7 Å in length with the carboxyl group of Asp99β2 and a few weaker intersubunit van der Waals contacts 3.5−4.0 Å in length with the guanidinium group of Arg40β2. In addition, a number of intrasubunit packing contacts of ≤4 Å occur between Tyr42α and Thr39α, Thr41α, Phe43α, Val93α, Asp94α, Asn97α, and the edge of the heme group. Included among these are a 3.0 Å hydrogen bond with the backbone NH group of Asp94α and a 3.3 Å hydrogen bond with the side chain of Asn97α. The side chain of Tyr42α1 also participates in an α1β2

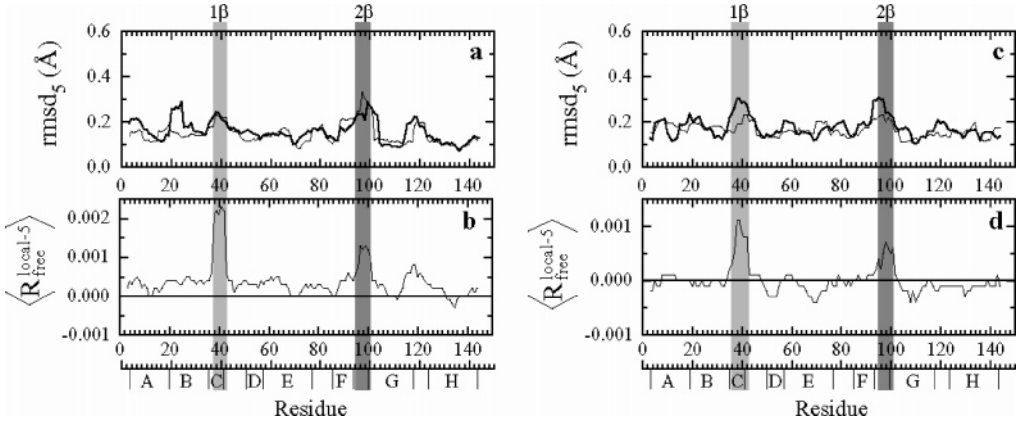

FIGURE 8: Plots of β-subunit rmsd$_5$ (a and c) and $\langle R_{free}^{local-5} \rangle$ (b and d) profiles for crystal form 2 (a and b) and crystal form 1 (c and d), where each parameter has been calculated over all overlapping five-residue windows. In panels a and c, the β1 and β2 subunit profiles are drawn with thin and thick lines, respectively. The globin helical boundaries are indicated along the bottom axis. The gray bands (labeled 1β and 2β) highlight the two $\langle R_{free}^{local-5} \rangle$ peaks in panels b and d.

intersubunit water bridge; the water molecule (labeled w1 in Figure 9) is positioned 2.9 Å from the hydroxyl group of Tyr42α1 and 3.0 Å from the amide side chain of Asn102β2.

Elimination of the phenolic group of Tyr42α ruptures all of the contacts mentioned above and creates a large cavity at the center of the quaternary-T α1β2 interface in deoxy αY42A. As illustrated in Figure 9 (where the α-subunits of αY42A and deoxy HbA have been superimposed), most of the α1 subunit atoms that were in contact with the side chain of Tyr42α1 move toward the cavity in an attempt to fill the newly created void. These movements correspond to features 1α and 2α in Figure 7, the largest mutation-induced tertiary structure changes in deoxy αY42A. The small shifts seen in the β2 subunit in Figure 9 are a combination of the very small tertiary structure changes 1β and 2β identified in Figure 8 and a very small change in quaternary structure. (Rigid-body analysis revealed a 0.3° mutation-induced rotation of the α1β1 dimer relative to the α2β2 dimer.) In addition to the changes in atomic positions, the αY42A mutation results in significant increases in the average atomic temperature factors for the side chains of residues Val93α, Asp94α, Asn97α, Arg40β, and Asp99β as well as for the bridging water molecule (w1 in Figure 9). The temperature factors of these side chains and water w1, which are in contact with Tyr42α, increase by a factor of ∼2. There is also a 0.1−0.2 Å increase in length for the Asp94α−Trp37β and Asn97α−Asp99β hydrogen bonds located near the αY42A mutation site, suggesting these hydrogen bonds are weakened in deoxy αY42A.

DISCUSSION

The Tyr42α1−Asp99β2 interaction occurs at the center of the α1β2 interface in the quaternary-T structure of deoxyhemoglobin, where the hydrogen bond between Tyr42α1 and Asp99β2 has been hypothesized to be an important quaternary-T constraint (*76*, *77*). This hypothesis was supported by studies on two site-directed mutant hemoglobins, αY42F and αY42H (*15*−*18*). In contrast to the cooperative αY42H mutant that had an only slightly elevated ligand affinity and formed a His42α1−Asp99β2 hydrogen bond, the αY42F mutant, which cannot form a hydrogen bond with Asp99α, was found to be noncooperative and to have very high ligand affinity. Spectroscopic evidence indicated that deoxy αY42F has a tertiary structure similar to that of fully

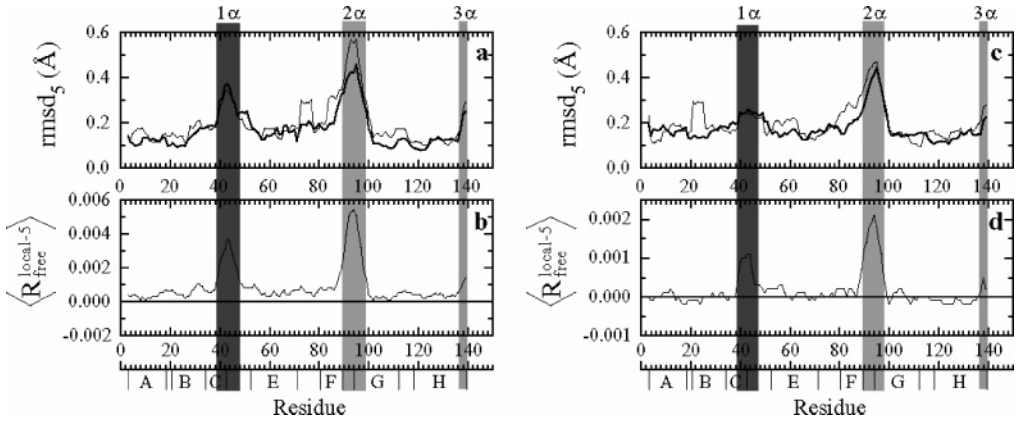

FIGURE 7: Plots of α-subunit rmsd$_5$ (a and c) and $\langle R_{free}^{local-5} \rangle$ (b and d) profiles for crystal form 2 (a and b) and crystal form 1 (c and d), where each parameter has been calculated over all overlapping five-residue windows (see the text). The rmsd$_5$ parameter is the root-mean-square deviation in α-subunit atomic coordinates calculated after a deoxy αY42A α-subunit has been superimposed via the sieve-fit protocol (see Materials and Methods) onto the corresponding deoxy HbA α-subunit. The $\langle R_{free}^{local-5} \rangle$ profile cross-validates tertiary structure changes and is described in the text. In panels a and c, the α1 and α2 subunit profiles are drawn with thin and thick lines, respectively. The globin helical boundaries are indicated along the bottom axis. The colored bands (labeled 1α−3α) highlight the three major $\langle R_{free}^{local-5} \rangle$ peaks in panels b and d.

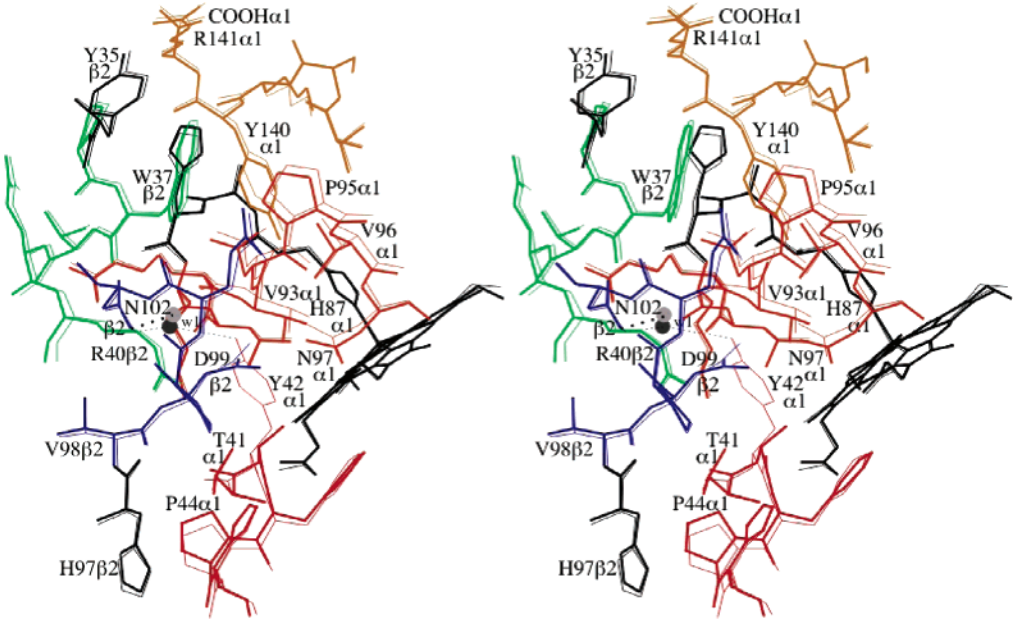

FIGURE 9: Stereo figure showing the environment in crystal form 2 of residue 42α1 in deoxy HbA (thin lines) and deoxy αY42A (thick lines) after the α1 subunits were superimposed using the sieve-fit procedure. The color coding corresponds to the polypeptide segments identified by the $\langle R_{free}^{local-5} \rangle$ profiles in Figures 7a and 8a. Water molecule w1 is shown as dark and light spheres for deoxy HbA and deoxy αY42A, respectively. Hydrogen bonds to water w1 are represented by dotted lines. An analogous stereo figure (not shown) for crystal form 1 structures of deoxy HbA and deoxy αY42A shows the same mutation-induced structural changes as those shown for crystal form 2.

liganded HbA, and this was interpreted as indicating that deoxy αY42F has a quaternary structure similar to that of fully liganded HbA and is incapable of adopting the quaternary-T structure of deoxy HbA (*15*, *16*). Thus, Ishimori et al. (*15*) concluded that, "the hydrogen bond formed between Tyr42α and Asp99*β* is required to convert unliganded hemoglobin to the T-state", and Imai et al. (*16*) stated that, "the hydrogen bond between Tyr42α and Asp99*β* plays a key role in stabilizing the deoxy T structure and consequently in cooperative oxygen binding".

However, removal of just the OH group of Tyr42α buries a very hydrophobic phenylalanine side chain next to the side chain of Asp99*β*, which has been shown to be negatively charged in quaternary-T hemoglobin (*78*). Thus, in addition to eliminating the Tyr42α1−Asp99*β*2 hydrogen bond, the αY42F mutation places the side chains of both Asp99*β* and Phe42α in very unfavorable environments, shifting the T−R^e equilibrium in favor of the R^e ensemble and/or forcing the dissociation of the hemoglobin tetramer to free α*β* dimers. In contrast, the αY42A mutation creates a cavity that is large enough to allow Asp99*β* to be hydrated and leaves the *β*-methyl group of Ala42α in the same environment as the *β*-methylene group of Tyr42α (i.e., packed against the edge of the α−heme group). Thus, it is reasonable to assume that removing the Tyr42α1−Asp99*β*2 hydrogen bond in the αY42A mutant will have a much weaker destabilizing impact on the quaternary-T tetramer than removing the Tyr42α1−Asp99*β*2 hydrogen bond in the αY42F mutant. This hypothesis is supported by the functional, spectroscopic, and crystallographic studies on αY42A reported above, which demonstrate that a quaternary-T structure, with only moderately increased ligand affinity, can be formed in the absence of the Tyr42α1−Asp99*β*2 hydrogen bond. Thus, the Tyr42α1−Asp99*β*2 hydrogen bond is not a major quaternary constraint, and its role in hemoglobin's stereochemical mechanism of action is much less important than previously proposed.

Two Crystal Structures of Deoxy αY42A Exhibit Only Small Mutation-Induced Perturbations. The two independent crystal structures of deoxy αY42A described above clearly show that the elimination of the phenolic side chain of Tyr42α does not greatly perturb the quaternary or tertiary structure of deoxyhemoglobin. The αY42A mutation, which creates a large cavity in the α1*β*2 interface, still results in an only 0.3° rotation of the α1*β*1 dimer relative to the α2*β*2 dimer and in small tertiary structure changes of a few tenths of an angstrom.

It is interesting to compare the small structural changes in deoxy αY42A with those generated by mutations at residue Trp37*β*, another residue whose bulky side chain is buried in the α1*β*2 interface where it makes both polar and nonpolar intersubunit interactions. Like the αY42A mutation, the *β*W37A and *β*W37G mutations create large cavities that diminish the stereochemical complementarity of the α1*β*2 interface. However, in deoxy *β*W37A and deoxy *β*W37G, the α1*β*1 dimer rotates relative to the α2*β*2 dimer by 1.0° and 2.0°, respectively (*46*). While mutations at positions 42α and 37*β* result in small, but valid, tertiary structure changes that involve many of the same atoms located at the α1*β*2 interface, there are important differences in the nature of the tertiary structure changes in αY42A and those observed in the 37*β* variants. For both mutation sites, the largest change in tertiary structure involves movement of residues in the α-subunit FG corner−G helix region that correspond to cross-validated feature 2α in Figure 7. However, the mutation-induced shifts of the atoms in this region of the α-subunit are in opposite directions in αY42A and the 37*β* variants. Specifically, in αY42A, the atoms associated with feature 2α shift toward the cavity created at the α1*β*2 interface, reducing the size of the cavity. This is a typical

response to cavity formation that has been observed in several crystallographic studies of mutations that create internal cavities in small, monomeric globular proteins (*79*−*81*). In contrast, mutations at position 37β induce shifts of atoms in the α-subunit FG corner−G helix region that are directed away from the mutation site, enlarging the size of the cavity (*46*). Another difference in the tertiary structure changes in the 37β mutants versus those in αY42A involves the C-terminal dipeptide of the α−subunit. In deoxy αY42A, there are only small shifts in this region (feature 3α in Figure 7), whereas this region exhibits large changes in position and mobility in the deoxy structures of the 37β mutants. As discussed below, the differences in the structural response to mutations at Tyr42α and Trp37β suggest that in deoxyhemoglobin interactions associated with Trp37β create tension at the α1β2 interface that extends to the heme groups, whereas the interactions associated with Tyr42α induce little if any tension.

Mutation-Induced Changes in the Stability of the Unliganded Hemoglobin Tetramer in Solution. The kinetics of combination of CO with αY42A reveals a number of effects of this mutation on the functional properties of the hemoglobin molecule, some obvious and others requiring some analysis to discern. In the presence of IHP, this mutant exhibits normal kinetic cooperativity, i.e., autocatalysis, but reacts with CO at roughly twice the rate of HbA. Because of the strong correlation between the CO combination rate and the ligand affinity of quaternary-T hemoglobin in the presence of IHP (*59*−*61*), it is possible to estimate that the ligand affinity of the deoxygenated quaternary αY42A tetramer is increased by approximately 2.5-fold. This increase is not insignificant but seems to be a minor effect when compared to the greater than 50-fold increase in the affinity of the quaternary T state resulting from the βW37A mutation. In the absence of IHP, one observes a rapid kinetic phase representing roughly 10% of the total reaction. However, this rapid kinetic process is unlikely to originate from the presence of quaternary-R^e tetramers in equilibrium with quaternary-T tetramers because the rate of establishment of the R^e−T equilibrium is in general much faster than the rates of CO binding under our experimental conditions (a situation that would result in a single kinetic phase). On the other hand, the equilibrium between tetrameric hemoglobin molecules and $\alpha\beta$ dimers relaxes at a much slower rate, supporting the assignment of the rapid process to the combination of CO with $\alpha\beta$ dimers. This assignment is further supported by the elimination of the rapid process by chemically cross-linking the hemoglobin tetramers, or by the addition of IHP that binds preferentially to the deoxygenated quaternary-T tetramer. The presence of $\alpha\beta$ dimers in the absence of IHP indicates destabilization of the deoxygenated hemoglobin tetramer by the αY42A substitution. Using a total heme concentration of 4 μM before mixing, the equilibrium constant for the assembly of deoxygenated $\alpha\beta$ dimers into tetramers can be calculated to be 36×10^6 M^{-1}. This indicates a standard free energy of tetramer assembly ($\Delta G°$) of −10 kcal/mol. According to Ackers et al. (*9*), the assembly free energy of deoxygenated HbA at pH 7.4 and 21.5 °C is −14.3 kcal/mol. Atha and Riggs (*82*) measured the pH dependence of the dimer−tetramer equilibrium of human HbA and found that between pH 7.4 and 7.0 the standard free energy for the assembly of deoxygenated $\alpha\beta$ dimers in forming the deoxygenated HbA tetramer becomes more negative by 0.6 kcal/mol. If one ignores the effect of a 1.5 °C change in temperature, this suggests that the αY42A substitution destabilizes the deoxygenated hemoglobin tetramer by some 4.9 kcal/mol. However, at pH 7.4 in the absence of IHP, the oxygen-saturated HbA tetramer is destabilized relative to the unliganded tetramer by 6.3 kcal/mol (*9*). Using the data of Atha and Riggs (*82*), one can estimate that at pH 7 this free energy difference is increased to 7.2 kcal/mol. Therefore, if the stability of the unliganded R^e quaternary state is similar to that of the liganded R^e quaternary state, this mutant would exist primarily as quaternary-T tetramers, even if the αY42A mutation had no effect on the stability of R^e tetramers. On the other hand, the presence of $\alpha\beta$ dimers in equilibrium with the deoxygenated T state of αY42A requires the presence of a small percentage of R^e state tetramers, sufficient to satisfy the dimer−R^e equilibrium. The free energy of assembly of unliganded $\alpha\beta$ dimers into R^e tetramers is not known, but it is reasonable to suspect the presence of 1 or 2% of such high-affinity tetramers. These R^e tetramers would have no significant effect on any of the other measurements reported here. However, the rate of CO combination with the deoxygenated tetramer is the sum of the products of the rate constants and the concentrations of each component of the tetramer population. Because of the very rapid rate at which CO combines with R^e state tetramers, they would contribute significantly to the rate at which CO combines with deoxygenated αY42A even if present at very low concentrations. Therefore, addition of IHP to deoxygenated αY42A would have the effect of assembling all of the $\alpha\beta$ dimers into tetramers and shifting the tetramer equilibrium to essentially 100% quaternary T. This might account for the fact that IHP has a greater effect on the rate of binding of CO to αY42A than to HbA.

Effect of the αY42A Mutation on the Overall Oxygen Affinity of Hemoglobin. The limited number of oxygen equilibria results reported here are sufficient to confirm that the αY42A variant forms hemoglobin tetramers, which bind oxygen cooperatively. The overall oxygen affinity at pH 7 is increased by a factor of approximately 3, both in the absence and in the presence of IHP. This is a greater increase than can be explained by a 2.5-fold increase in the oxygen affinity of the T quaternary state alone, but is consistent with a significant effect of the mutation on the stability of the quaternary T state and a resulting shift in the T−R^e equilibrium.

Solution Phase Quaternary Structure of αY42A. The deoxy minus CO UV resonance Raman difference spectrum for αY42A displays features that have been associated with the deoxy-to-liganded quaternary structure difference. In particular, the behaviors of the peak at 1550 cm^{-1} (which corresponds to the Trp37β contribution to W3) and the 1511 cm^{-1} peak (also associated with Trp37β) are indicative of a deoxy-to-liganded quaternary structure difference in the hinge region of the α1β2 interface that is similar to that which is observed for HbA. The strong derivative-shaped feature seen for HbA in the Y8a region (Figures 5 and 6) is not seen in the difference spectrum of the mutant. This difference feature has been directly linked to the formation of the hydrogen bond between Tyr42α and Asp99β in deoxy HbA (*14*, *71*, *72*). Thus, it is not surprising that it is missing in the

difference spectrum of αY42A as it was from the corresponding difference spectrum of the βD99N/αY42D double mutant (*14*). These results, in conjunction with the oxygen binding titrations that show that αY42A is cooperative, indicate that the deoxy-to-liganded quaternary changes associated with both ligand reactivity and conformation at the hinge region of the α1β2 interface can occur in the complete absence of the Tyr42α−Asp99β hydrogen bond.

It can also be seen from the detailed comparisons between HbA and αY42A that despite the near-normal functioning of the hinge region, the local environment about Trp37β is altered as reflected in the slight mutation-induced changes in the shoulder of W3 in the UV resonance Raman spectrum. These spectra were taken at high-protein concentration conditions in the presence of IHP, two factors that minimize the contribution of dimers. Under all conditions used to generate the Raman spectra, IHP has no impact on the spectra from the deoxy derivatives. As will be discussed in a subsequent section, these changes, albeit small, are likely reflective of the specific conformational differences that give rise to the altered tetramer properties of this mutant.

Solution Phase Conformations of αY42A: Tertiary Structure at the Heme. The frequency of ν(Fe−His) is highly sensitive to the details of subunit tertiary structure, which respond to ligation, quaternary structure, and allosteric effectors (*28*, *29*, *31*, *33*−*38*, *83*−*86*). In general, the frequency of ν(Fe−His) for the deoxy derivative increases upon going from the T to the R^e structures. Within the quaternary-T structure or the quaternary-R^e ensemble, the frequency increases upon going from the deoxy derivative to the transient five-coordinate species generated within a few nanoseconds of photodissociation of the liganded derivative. For the photoproducts, the frequency increases upon going from ligated T to ligated R^e. For a given ligated species, the addition of allosteric effectors typically lowers the frequency of ν(Fe−His). Thus, for HbA, the deoxy quaternary-T species and the photoproduct quaternary-R^e species represent the low (214 cm^{-1}) and high (230 cm^{-1}) end points for the frequency of ν(Fe−His). Whereas for the end point frequencies there is little if any uncertainty assigning quaternary structure, the conformational assignment remains ambiguous for solutions that yield intermediate frequencies. For example, a frequency in the range of 218−225 cm^{-1} could arise from either R^e or T. The frequency of ν(Fe−His) for deoxy αY42A is at most 1 cm^{-1} higher than the low end point value seen for deoxy HbA. This frequency for deoxy αY42A is consistent with a quaternary-T species.

Stereochemical Linkage among Tyr42α1, Trp37β2, and the α1-Heme Group. Recent research has demonstrated that the major region of quaternary-T constraint is located in a cluster of α1β2 interface residues centered at Trp37β and termed the "Trp37β cluster". In particular, Noble et al. (*26*) conducted an extensive alanine mutagenic screen of the dimer−dimer interface and found that the low ligand affinity of deoxyhemoglobin is most sensitive to mutations at Trp37β and those residues in contact with Trp37β. The relationship between the atomic interactions associated with the Trp37β cluster and the functional and spectroscopic properties of deoxy HbA emerged from extensive collaborative studies on a series of 37β mutants (*21*, *28*, *46*, *87*). In these studies, it was observed that in the deoxy state the βW37Y, βW37A, βW37G, and βW37E mutants manifest a range of T-like quaternary structures and a range of tertiary conformations at the Trp37β cluster. In particular, Tyr140α shows a progressive increase in the level of disorder for the Tyr, Ala, Gly, and Glu mutations (*46*). The distribution of tertiary conformations associated with the packing of the α-subunit C-terminus corresponds to a distribution of proximal heme environments as reflected in a 214−218 cm^{-1} spread in the frequency of ν(Fe−His) (*28*). Specifically, an increased level of disorder at the C-terminus correlates with decreased proximal strain as reflected in an increase in the frequency of ν(Fe−His). Very recent crystallographic studies on quaternary-T nitrosylhemoglobin also demonstrate a direct linkage between the quaternary constraints associated with Trp37β and the Fe−His bond (*48*). When crystals of wild-type deoxyhemoglobin are exposed to NO, the α (but not the β) Fe−His bond is broken. In contrast, when crystals of βW37E deoxyhemoglobin are exposed to NO, both the α and β Fe−His bonds remain intact, indicating that ligand-induced strain at the α Fe−His bond is greatly reduced when the quaternary constraints associated with Trp37β are eliminated by mutation. Other spectroscopic studies on Fe−Zn hybrid forms of HbA (*37*), sol−gel encapsulation studies on HbA (*88*), and variant hemoglobins with altered α C-termini (*86*, *89*) also show that ligand binding within the quaternary-T structure induces tertiary structure changes that increase the frequency of ν(Fe−His) from 214 cm^{-1} to values ranging from 217 to 224 cm^{-1}.

The crystal structures of αY42A as well as the UV resonance Raman spectra show that removing the Tyr42α1−Asp99β2 hydrogen bond and the other interactions associated with the phenolic side chain of Tyr42α results in small structural changes to the environment of Trp37β. In particular, the length of the Trp37β2−Asp94α1 hydrogen bond increases by ∼0.15 Å and Tyr140α (the α C-terminal penultimate tyrosine which is in contact with Trp37β) shifts slightly (Figure 9 and feature 3α in Figure 7). The evidence presented above indicates that these small structural changes are the stereochemical basis for the small increase in the frequency of ν(Fe−His) and the modest increase in the ligand affinity of deoxy αY42A.

Stability versus Affinity for the Quaternary-T Tetramer. If one or more of hemoglobin's major quaternary-T constraints are eliminated by mutation, a correspondingly substantial increase in the ligand affinity of the quaternary-T state of the mutant hemoglobin tetramer must also occur. This linkage is the case for mutations at residue Trp37β (*21*, *26*, *28*, *46*, *87*), which have been shown to increase the ligand affinity of the quaternary-T tetramer. Alternatively, an interaction across the α1β2 interface may serve to stabilize the T state tetramer with respect to dissociation into αβ dimers without having a direct effect on the ligand affinity of the quaternary-T state. If such an interaction is found only in the quaternary-T state, being absent from the ensemble of R state structures, then the elimination of the interaction by mutation will shift the T−R^e equilibrium in favor of the R^e states. This shift will increase the *overall* ligand affinity of the mutant hemoglobin without necessarily having an effect on the ligand binding properties of the T state. The interactions associated with Tyr42α are primarily of this type.

REFERENCES

1. Fermi, G., Perutz, M. F., Shaanan, B., and Fourme, R. (1984) The crystal structure of human deoxyhaemoglobin at 1.74 Å resolution, *J. Mol. Biol. 175*, 159−174.
2. Kavanaugh, J. S., Rogers, P. H., Case, D. A., and Arnone, A. (1992) High-resolution X-ray study of deoxyhemoglobin Rothschild 37β Trp → Arg: A mutation that creates an intersubunit chloride-binding site, *Biochemistry 31*, 4111−4121.
3. Kavanaugh, J. S., Moo-Penn, W. F., and Arnone, A. (1993) Accommodation of insertions in helices: The mutation in hemoglobin Catonsville (Pro 37α-Glu-Thr 38α) generates a $3_{(10)}$ → α bulge, *Biochemistry 32*, 2509−2513.
4. Mueser, T. C., Rogers, P. H., and Arnone, A. (2000) Interface sliding as illustrated by the multiple quaternary structures of liganded hemoglobin, *Biochemistry 39*, 15353−15364.
5. Shaanan, B. (1983) Structure of human oxyhaemoglobin at 2.1 Å resolution, *J. Mol. Biol. 171*, 31−59.
6. Silva, M. M., Rogers, P. H., and Arnone, A. (1992) A third quaternary structure of human hemoglobin A at 1.7-Å resolution, *J. Biol. Chem. 267*, 17248−17256.
7. Lukin, J. A., Kontaxis, G., Simplaceanu, V., Yuan, Y., Bax, A., and Ho, C. (2003) Quaternary structure of hemoglobin in solution, *Proc. Natl. Acad. Sci. U.S.A. 100*, 517−520.
8. Monod, J., Wyman, J., and Changeux, J.-P. (1965) On the nature of allosteric transitions: A plausible model, *J. Mol. Biol. 12*, 88−118.
9. Ackers, G. K., Holt, J. M., Huang, Y., Grinkova, Y., Klinger, A. L., and Denisov, I. (2000) Confirmation of a unique intra-dimer cooperativity in the human hemoglobin α1β1 half-oxygenated intermediate supports the symmetry rule model of allosteric regulation, *Proteins Suppl. 4*, 23−43.
10. Perutz, M. F., Wilkinson, A. J., Paoli, M., and Dodson, G. G. (1998) The stereochemical mechanism of the cooperative effects in hemoglobin revisited, *Annu. Rev. Biophys. Biomol. Struct. 27*, 1−34.
11. Turner, G. J., Galaceros, F., Doyle, M. L., Hedlund, B., Pettigrew, D. W., Turner, B. W., Smith, F. R., Moo-Penn, W., Rucknagel, D. L., and Ackers, G. K. (1992) Mutagenic dissection of hemoglobin cooperativity: Effects of amino acid alteration on subunit assembly of oxy and deoxy tetramers, *Proteins 14*, 333−350.
12. Doyle, M. L., Lew, G., Turner, G. J., Rucknagel, D., and Ackers, G. K. (1992) Regulation of oxygen affinity by quaternary enhancement: Does hemoglobin Ypsilanti represent an allosteric intermediate? *Proteins 14*, 351−362.
13. Kim, H. W., Shen, T. J., Sun, D. P., Ho, N. T., Madrid, M., Tam, M. F., Zou, M., Cottam, P. F., and Ho, C. (1994) Restoring allosterism with compensatory mutations in hemoglobin, *Proc. Natl. Acad. Sci. U.S.A. 91*, 11547−11551.
14. Huang, S., Peterson, E. S., Ho, C., and Friedman, J. M. (1997) Quaternary structure sensitive tyrosine interactions in hemoglobin: A UV resonance Raman study of the double mutant rHb (β99Asp→Asn, α42Tyr→Asp), *Biochemistry 36*, 6197−6206.
15. Ishimori, K., Morishima, I., Imai, K., Fushitani, K., Miyazaki, G., Shih, D., Tame, J., Pegnier, J., and Nigai, K. (1989) NMR study of human mutant hemoglobins synthesized in *Escherichia coli*: Consequences of tyrosine α42 substitutions, *J. Biol. Chem. 264*, 14624−14626.
16. Imai, K., Fushitani, K., Miyazaki, G., Ishimori, K., Kitagawa, T., Wada, Y., Morimoto, H., Morishima, I., Shih, D. T., and Tame, J. (1991) Site-directed mutagenesis in haemoglobin: Functional role of tyrosine-42(C7)α at the α1-β2 interface, *J. Mol. Biol. 218*, 769−778.
17. Togi, A., Ishimori, K., Unno, M., Konno, T., Morishima, I., Miyazaki, G., and Imai, K. (1993) Effects of intra- and intersubunit hydrogen bonds on the R−T transition in human hemoglobin as studied with α42(C7) and β145(HC2) mutations, *Biochemistry 32*, 10165−10169.
18. Tame, J. R., and Vallone, B. (2000) The structures of deoxy human haemoglobin and the mutant Hb Tyrα42His at 120 K, *Acta Crystallogr. D56*, 805−811.
19. Hernan, R. A., Hui, H. L., Andracki, M. E., Noble, R. W., Sligar, S. G., Walder, J. A., and Walder, R. Y. (1992) Human hemoglobin expression in *Escherichia coli*: Importance of optimal codon usage, *Biochemistry 31*, 8619−8628.
20. Hui, H. L., Kavanaugh, J. S., Doyle, M. L., Wierzba, A., Rogers, P. H., Arnone, A., Holt, J. M., Ackers, G. K., and Noble, R. W. (1999) Structural and functional properties of human hemoglobins reassembled after synthesis in *Escherichia coli*, *Biochemistry 38*, 1040−1049.
21. Kwiatkowski, L. D., Hui, H. L., Wierzba, A., Noble, R. W., Walder, R. Y., Peterson, E. S., Sligar, S. G., and Sanders, K. E. (1998) Preparation and kinetic characterization of a series of βW37 variants of human hemoglobin A: Evidence for high-affinity T quaternary structures, *Biochemistry 37*, 4325−4335.
22. Chatterjee, R., Welty, E. V., Walder, R. Y., Pruitt, S. L., Rogers, P. H., Arnone, A., and Walder, J. A. (1986) Isolation and characterization of a new hemoglobin derivative cross-linked between the α chains (Lysine 99α1 → Lysine 99α2), *J. Biol. Chem. 261*, 9929−9937.
23. Snyder, S. R., Welty, E. V., Walder, R. Y., Williams, L. A., and Walder, J. A. (1987) HbXL99α: A hemoglobin derivative that is cross-linked between the α subunits is useful as a blood substitute, *Proc. Natl. Acad. Sci. U.S.A. 84*, 7280−7284.
24. Riggs, A. (1981) Preparation of blood hemoglobins of vertebrates, *Methods Enzymol. 76*, 5−29.
25. Doyle, M. L., Lew, G., De Young, A., Kwiatkowski, L., Wierzba, A., Noble, R. W., and Ackers, G. K. (1992) Functional properties of human hemoglobins synthesized from recombinant mutant β-globins, *Biochemistry 31*, 8629−8639.
26. Noble, R. W., Hui, H. L., Kwiatkowski, L. D., Paily, P., DeYoung, A., Wierzba, A., Colby, J. E., Bruno, S., and Mozzarelli, A. (2001) Mutational effects at the subunit interfaces of human hemoglobin: Evidence for a unique sensitivity of the T quaternary state to changes in the hinge region of the α1β2 interface, *Biochemistry 40*, 12357−12368.
27. Hayashi, A., Suzuki, T., and Shin, M. (1973) An enzymic reduction system for metmyoglobin and methemoglobin, and its application to functional studies of oxygen carriers, *Biochim. Biophys. Acta 310*, 309−316.
28. Peterson, E. S., and Friedman, J. M. (1998) A possible allosteric communication pathway identified through a resonance Raman study of four β37 mutants of human hemoglobin A, *Biochemistry 37*, 4346−4357.
29. Friedman, J. M., Scott, T. W., Stepnoski, R. A., Ikeda-Saito, M., and Yonetani, T. (1983) The iron-proximal histidine linkage and protein control of oxygen binding in hemoglobin: A transient Raman study, *J. Biol. Chem. 258*, 10564−10572.
30. Friedman, J. M., Rousseau, D. L., Ondrias, M. R., and Stepnoski, R. A. (1982) Transient Raman study of hemoglobin: Structural dependence of the iron-histidine linkage, *Science 218*, 1244−1246.
31. Friedman, J. M. (1985) Structure, dynamics, and reactivity in hemoglobin, *Science 228*, 1273−1280.
32. Jayaraman, V., Rodgers, K. R., Mukerji, I., and Spiro, T. G. (1995) Hemoglobin allostery: Resonance Raman spectroscopy of kinetic intermediates, *Science 269*, 1843−1848.
33. Kitagawa, T. (1988) in *Biological Application of Raman Spectroscopy* (Spiro, T. G., Ed.) pp 97−131, Wiley & Sons, New York.
34. Ondrias, M. R., Rousseau, D. L., Shelnutt, J. A., and Simon, S. R. (1982) Quaternary-transformation-induced changes at the heme in deoxyhemoglobins, *Biochemistry 21*, 3428−3437.
35. Samuni, U., Dantsker, D., Khan, I., Friedman, A. J., Peterson, E., and Friedman, J. M. (2002) Spectroscopically and kinetically distinct conformational populations of sol−gel-encapsulated carbonmonoxy myoglobin: A comparison with hemoglobin, *J. Biol. Chem. 277*, 25783−25790.
36. Hu, X., Rodgers, K. R., Mukerji, I., and Spiro, T. G. (1999) New light on allostery: Dynamic resonance Raman spectroscopy of hemoglobin Kempsey, *Biochemistry 38*, 3462−3467.
37. Samuni, U., Juszczak, L., Dantsker, D., Khan, I., Friedman, A. J., Perez-Gonzalez-de-Apodaca, J., Bruno, S., Hui, H. L., Colby, J. E., Karasik, E., Kwiatkowski, L. D., Mozzarelli, A., Noble, R., and Friedman, J. M. (2003) Functional and spectroscopic characterization of half-liganded iron−zinc hybrid hemoglobin: Evidence for conformational plasticity within the T state, *Biochemistry 42*, 8272−8288.
38. Rousseau, D. L., and Friedman, J. M. (1988) in *Biological Applications of Raman Spectroscopy* (Spiro, T. G., Ed.) pp 133−215, Wiley & Sons, New York.
39. Huang, J., Juszczak, L. J., Peterson, E. S., Shannon, C. F., Yang, M., Huang, S., Vidugiris, G. V., and Friedman, J. M. (1999) The conformational and dynamic basis for ligand binding reactivity in hemoglobin Ypsilanti (β99 Asp→Tyr): Origin of the quaternary enhancement effect, *Biochemistry 38*, 4514−4525.

40. Juszczak, L. J., and Friedman, J. M. (1999) UV resonance Raman spectra of ligand binding intermediates of sol−gel encapsulated hemoglobin, *J. Biol. Chem. 274*, 30357−30360.
41. Juszczak, L. J., Fablet, C., Baudin-Creuza, V., Lesecq-Le Gall, S., Hirsch, R. E., Nagel, R. L., Friedman, J. M., and Pagnier, J. (2003) Conformational changes in hemoglobin S (βE6V) imposed by mutation of the β Glu7β-Lys132 salt bridge and detected by UV resonance Raman spectroscopy, *J. Biol. Chem. 278*, 7257−7263.
42. Perutz, M. F. (1968) Preparation of haemoglobin crystals, *J. Cryst. Growth 2*, 54−56.
43. Ward, K. B., Wishner, B. C., Lattman, E. E., and Love, W. E. (1975) Structure of deoxyhemoglobin A crystals grown from polyethylene glycol solutions, *J. Mol. Biol. 98*, 161−177.
44. Jancarik, J., and Kim, S. H. (1991) Sparse matrix sampling: A screening method for crystallization of proteins, *J. Appl. Crystallogr. 24*, 409−411.
45. Cudney, R., Patel, S., Weisgraber, K., Newhouse, Y., and McPherson, A. (1994) Screening and optimization strategies for macromolecular crystal growth, *Acta Crystallogr. D50*, 414−423.
46. Kavanaugh, J. S., Weydert, J. A., Rogers, P. H., and Arnone, A. (1998) High-resolution crystal structures of human hemoglobin with mutations at tryptophan 37β: Structural basis for a high-affinity T-state, *Biochemistry 37*, 4358−4373.
47. Howard, A. J., Nielsen, C., and Xuong, N. H. (1985) Software for a diffractometer with multiwire area detector, *Methods Enzymol. 114*, 452−472.
48. Chan, N.-L., Kavanaugh, J. S., Rogers, P. H., and Arnone, A. (2004) Crystallographic analysis of the interaction of nitric oxide quaternary-T human hemoglobin, *Biochemistry 43*, 118−132.
49. Brünger, A. T. (1993) Assesment of phase accuracy by cross validation: The Free R Value. Methods and Applications, *Acta Crystallogr. D49*, 24−36.
50. Murshudov, G., Vagin, A. A., and Dodson, E. J. (1997) Refinement of molecular structures by the maximum-likelihood method, *Acta Crystallogr. D53*, 240−255.
51. Collaborative Computational Project No. 4 (1994) *Acta Crystallogr. D50*, 760−763.
52. Brünger, A. T. (1992) *X-PLOR*, version 3.1, Yale University Press, New Haven, CT.
53. Jones, T. A. (1985) Diffraction methods for biological macromolecules. Interactive computer graphics: FRODO, *Methods Enzymol. 115*, 157−171.
54. Cambillau, C. (1989) *Silicon Graphics Geometry Partners Directory*, p 61, Silicon Graphics, Mountain View, CA.
55. Brünger, A. T. (1992) Free R-value: A novel statistical quantity for assessing the accuracy of crystal structures, *Nature 355*, 472−474.
56. Gerstein, M., and Chothia, C. (1991) Analysis of protein loop closure: Two types of hinges produce one motion in lactate dehydrogenase, *J. Mol. Biol. 220*, 133−149.
57. Cox, J. M. (1967) Mathematical methods used in the comparison of the quaternary structures, *J. Mol. Biol. 28*, 151−156.
58. Fowler, S. A., Walder, J., DeYoung, A., Kwiatkowski, L. D., and Noble, R. W. (1992) Isolation and characterization of the triply oxidized derivative of a cross-linked hemoglobin, *Biochemistry 31*, 717−725.
59. Noble, R. W., Kwiatkowski, A. V., Hui, H. L., Bruno, S., Bettati, S., and Mozzarelli, A. (2002) Correlation of protein functional properties in the crystal and in solution: The case study of T-state hemoglobin, *Protein Sci. 11*, 1845−1849.
60. Hui, H. L., Kwiatkowski, L. D., Karasik, E., Colby, J. E., and Noble, R. W. (2004) Ligand binding to symmetrical Fe−Zn hybrids of variants of human HbA with modifications in the $\alpha 1\beta 2$ interface, *Biochemistry 43*, 7843−7850.
61. Karasik, E., Kwiatkowski, L. D., Hui, H. L., Colby, J. E., and Noble, R. W. (2004) Effects of heterotropic allosteric effectors on the equilibrium and kinetics of the reaction of a single ligand molecule with an α or β subunit of deoxygenated HbA, *Biochemistry 43*, 7851−7856.
62. Zhao, X., Chen, R., Raj, V., and Spiro, T. G. (2001) Assignment of the 1511 cm^{-1} UV resonance Raman marker band of hemoglobin to tryptophan, *Biopolymers 62*, 158−162.
63. Su, C., Park, Y. D., Liu, G., and Spiro, T. G. (1989) Hemoglobin quaternary structure change monitored directly by transient UV resonance Raman spectroscopy, *J. Am. Chem. Soc. 111*, 3457−3459.
64. Rodgers, K., Su, S., Subramaniam, S., and Spiro, T. (1992) Hemoglobin R→T structural dynamics from simultaneous monitoring of tyrosine and tryptophan time-resolved UV resonance Raman signals, *J. Am. Chem. Soc. 114*, 3697−3709.
65. Jayaraman, V., Rodgers, K. R., Mukerji, I., and Spiro, T. G. (1993) R and T states of fluoromethemoglobin probed by ultraviolet resonance Raman spectroscopy, *Biochemistry 32*, 4547−4551.
66. Samuni, U., Navati, M. S., Juszczak, L. J., Dantsker, D., Yang, M., and Friedman, J. M. (2000) Unfolding and refolding of sol−gel encapsulated carbonmonoxymyoglobin: An orchestrated spectroscopic study of intermediates and kinetics? *J. Phys. Chem. B 104*, 10802−10813.
67. Wang, D., Zhao, X., Shen, T. S., Ho, C., and Spiro, T. G. (1999) Role of interhelical H-bonds (W14−T67 and W15−S72) in the hemoglobin allosteric reaction path evaluated by UV resonance Raman spectroscopy of site mutants, *J. Am. Chem. Soc. 121*, 11197−11203.
68. Nagai, M., Kaminaka, S., Ohba, Y., Nagai, Y., Mizutani, Y., and Kitagawa, T. (1995) Ultraviolet resonance Raman studies of quaternary structure of hemoglobin using a tryptophan β37 mutant, *J. Biol. Chem. 270*, 1636−1642.
69. Rodgers, K. R., and Spiro, T. G. (1994) Nanosecond dynamics of the R→T transition in hemoglobin: Ultraviolet Raman studies, *Science 265*, 1697−1699.
70. Mukerji, I., and Spiro, T. G. (1994) Modeling the hemoglobin switchpoint with cyanomet valency hybrids: Raman spectroscopic probes of tertiary and quaternary structure, *Biochemistry 33*, 13132−13139.
71. Wang, D., Zhao, X., and Spiro, T. G. (2000) Chain selectivity of tyrosine contributions to hemoglobin static and time-resolved UVRR spectra in C isotopic hybrids, *J. Phys. Chem. A 104*, 4149−4152.
72. Nagai, M., Wajcman, H., Lahary, A., Nakatsukasa, T., Nagatomo, S., and Kitagawa, T. (1999) Quaternary structure sensitive tyrosine residues in human hemoglobin: UV resonance Raman studies of mutants at α140, β35, and β145 tyrosine, *Biochemistry 38*, 1243−1251.
73. Hu, X., and Spiro, T. G. (1997) Tyrosine and tryptophan structure markers in hemoglobin ultraviolet resonance Raman spectra: Mode assignments via subunit-specific isotope labeling of recombinant protein, *Biochemistry 36*, 15701−15712.
74. Austin, J. C., Rodgers, K. R., and Spiro, T. G. (1993) Protein structure from ultraviolet resonance Raman spectroscopy, *Methods Enzymol. 226*, 374−396.
75. Austin, J., Jordan, T., and Spiro, T. (1993) in *Biomolecular Spectroscopy Part A* (Hester, R. E., Ed.) pp 55−127, Wiley & Sons, New York.
76. Perutz, M. F., and TenEyck, L. F. (1972) Stereochemistry of cooperative effects in hemoglobin, *Cold Spring Harbor Symp. Quant. Biol. 36*, 295−310.
77. Perutz, M. F. (1987) in *Molecular Basis of Blood Diseases* (Stammatayanopoulos, G., Ed.) pp 127−178, Saunders, Philadelphia.
78. Hu, X., Dick, L. A., and Spiro, T. G. (1998) Fourier transform infrared evidence against Asp β99 protonation in hemoglobin: Nature of the Tyrα42-Aspβ99 quaternary H-bond, *Biochemistry 37*, 9445−9448.
79. Jackson, S. E., Moracci, M., elMasry, N., Johnson, C. M., and Fersht, A. R. (1993) Effect of cavity-creating mutations in the hydrophobic core of chymotrypsin inhibitor 2, *Biochemistry 32*, 11259−11269.
80. Eriksson, A. E., Baase, W. A., Zhang, X.-J., Heinz, D. W., Blaber, M., Baldwin, E. P., and Matthews, B. W. (1992) Response of a protein structure to cavity-creating mutations and its relation to the hydrophobic effect, *Science 255*, 178−183.
81. Xu, J., Baase, W. A., Baldwin, E., and Matthews, B. W. (1998) The response of T4 lysozyme to large-to-small substitutions within the core and its relation to the hydrophobic effect, *Protein Sci. 7*, 158−177.
82. Atha, D. H., and Riggs, A. (1976) Tetramer-dimer dissociation in hemoglobin and the Bohr effect, *J. Biol. Chem. 251*, 5537−5543.
83. Ondrias, M. R., Rousseau, D. L., Kitagawa, T., Ikeda-Saito, M., Inubushi, T., and Yonetani, T. (1982) Quaternary structure changes in iron−cobalt hybrid hemoglobins detected by resonance Raman scattering, *J. Biol. Chem. 257*, 8766−8770.
84. Friedman, J. M. (1994) Time-resolved resonance Raman spectroscopy as probe of structure, dynamics, and reactivity in hemoglobin, *Methods Enzymol. 232*, 205−231.
85. Scott, T. W., and Friedman, J. M. (1984) Tertiary-structure relaxation in hemoglobin: A transient Raman study, *J. Am. Chem. Soc. 106*, 5677−5687.

86. Wang, D., and Spiro, T. G. (1998) Structure changes in hemoglobin upon deletion of C-terminal residues, monitored by resonance Raman spectroscopy, *Biochemistry 37*, 9940−9951.
87. Kiger, L., Klinger, A. L., Kwiatkowski, L. D., De Young, A., Doyle, M. L., Holt, J. M., Noble, R. W., and Ackers, G. K. (1998) Thermodynamic studies on the equilibrium properties of a series of recombinant βW37 hemoglobin mutants, *Biochemistry 37*, 4336−4345.
88. Samuni, U., Dantsker, D., Khan, I., Friedman, A. J., Peterson, E., and Friedman, J. M. (2002) Spectroscopically and kinetically distinct conformational populations of sol−gel encapsulated carbonmonoxy myoglobin: A comparison with hemoglobin, *J. Biol. Chem. 277*, 25783−25790.
89. Wajcman, H., Kister, J., Galacteros, F., Spielvogel, A., Lin, M. J., Vidugiris, G. J., Hirsch, R. E., Friedman, J. M., and Nagel, R. L. (1996) Hb Montefiore (126(H9)Asp→Tyr); High oxygen affinity and loss of cooperativity secondary to C-terminal disruption, *J. Biol. Chem. 271*, 22990−22998.

BI0484670